

Microstructural Evolution of 9Cr-ODS and JLF-1 in a HIP Joint after Post-bond Heat Treatment

Haiying FU¹⁾, Takuya NAGASAKA^{1,2)}, and Takeo MUROGA^{1,2)}

¹⁾*SOKENDAI (The Graduate University for Advanced Studies), Toki, Gifu, JAPAN*

²⁾*National Institute for Fusion Science, Toki, Gifu, JAPAN*

(Received: 23 September 2014 / Accepted: 19 January 2015)

A joint of 9Cr-ODS and JLF-1 (9Cr-2W RAFM) was fabricated by hot isostatic pressing (HIP) at 1000°C for 3h under a pressure of 191MPa with a slow cooling rate. JLF-1 was hardened and 9Cr-ODS was softened after the HIP. By microstructure analysis, JLF-1 showed quenched martensitic phase with MX particles and high density dislocation tangles in the matrix, while 9Cr-ODS showed ferritic phase with low density of carbides and coarse carbides on grain boundaries. After post-bond heat treatment (PBHT) with normalization and tempering at a fast cooling rate, microstructure of both 9Cr-ODS and JLF-1 was recovered to the same with that before HIP. Both of them were tempered martensitic phase with laths, carbides, and dislocations.

Keywords: microstructure, 9Cr-ODS, JLF-1, hot isostatic pressing, post-bond heat treatment

1. Introduction

Oxide dispersion strengthened (ODS) ferritic steel is a kind of reduced activation ferritic/martensitic steel (RAFM) for fusion application because of its excellent high temperature mechanical properties [1]. When the material is applied to the first wall and structural component of fusion reactor blankets by joining to the conventional non-ODS RAFM, it would increase the application temperature of blanket significantly [2]. Thus, bonding technology of ODS with non-ODS RAFM steels is very important for the construction of an advanced fusion reactor in the future. Up to now, lots of techniques have been utilized for the bonding, such as electron beam welding [3], friction welding [4,5], diffusion bonding [6] etc. Unlike conventional melting-solidification bonding techniques, diffusion bonding such as hot isostatic pressing (HIP) is a solid-state process, and does not create molten zone for the joint. Thus degradation of microstructure and properties at the interface would be avoided or diminished [6]. In the previous work [7], ODS-RAFM steel, 9Cr-ODS, and non-ODS RAFM steel, JLF-1, were bonded by HIP at 1000°C for 3h under 191MPa. Post-bond heat treatment (PBHT) with normalization and tempering at a fast cooling rate was utilized to recover the hardness of both 9Cr-ODS and JLF-1 base metals to the level similar to that before HIP. In the previous results, the microstructure of the interface between 9Cr-ODS and JLF-1 was mainly studied. The interface was softened compared to the base metals, because the carbides at the interface are coarser than those in the base metals. A layer of grains with few MX particles

on the JLF-1 side at the interface appeared after HIP. While after PBHT, the few-particle layer disappeared, but normal tempered martensitic phase of $M_{23}C_6$ carbides and MX particles formed. For the application of the bonded materials to the fusion components, characterization of the property change of the base metals by the heating history is necessary in addition to that of the bonding interfaces. In this work, microstructure evolution of base metals of 9Cr-ODS and JLF-1 by the heating history is mainly investigated.

2. Materials and experiment

Materials used in this study were 9Cr-ODS and JLF-1. 9Cr-ODS was fabricated by mechanical alloying followed by extrusion and forging at 1150°C [8]. JLF-1 was made by vacuum induction melting (VIM), forging, and rolling [9]. The normalization was carried out at 1050°C for 1h with air cooling (AC), followed by tempering at 800°C for 1h for 9Cr-ODS, and at 780°C for 1h for JLF-1. The chemical composition of the materials is shown in Table 1.

Table 1 Chemical composition of 9Cr-ODS and JLF-1 (wt. %).

Material	C	Si	Mn	P	S	Cr	O
9Cr-ODS	0.14	0.06	0.09	<0.005	0.004	9.08	0.16
JLF-1	0.09	0.05	0.49	<0.003	0.0005	9.00	0.002

Material	W	V	Ta	Ti	Y	N
9Cr-ODS	1.97			0.23	0.29	0.013
JLF-1	1.98	0.20	0.083			0.015

The 9Cr-ODS disk used in this study was 5 mm thick and 24 mm in diameter. The JLF-1 blocks were 20 mm

author's e-mail: fu.haiying@ms.nifs.ac.jp, fuhy@swip.ac.cn

thick and 24 mm in diameter. The blocks were electro-polished to remove the contamination of the surfaces with etching solution of 13% HClO₄, 13% ethylene glycol monobutyl ether, and 74% acetic acid, at 15V below 5°C. After cleaned and dried, the 9Cr-ODS disk was sandwiched between two JLF-1 blocks and sealed into a soft steel capsule using electron-beam welding, and then hot isostatically pressed at 1000°C for 3h at 191MPa. The cooling rate of the HIP was 5°C per minute. Coupon specimens provided with the bonding interface in the center were machined for microstructure analysis and hardness test. PBHT was carried out for the joint by normalization at 1050°C for 1h and tempering at 720-820°C for 1h. The cooling rate after normalization and tempering was 34~36°C per minute. Fig. 1 depicts the HIP and the following PBHT procedure for the joint. Hardness tests were carried out at 300g for 30s for the base metals as-HIPed and after PBHT. Microstructural analysis by transmission electron microscopy (TEM) and scanning electron microscopy (SEM) was executed for the joint after electro-etching. The etching solution is also 13% HClO₄, 13% ethylene glycol monobutyl ether, and 74% acetic acid. More details about the experimental procedure are shown in the previous work [7].

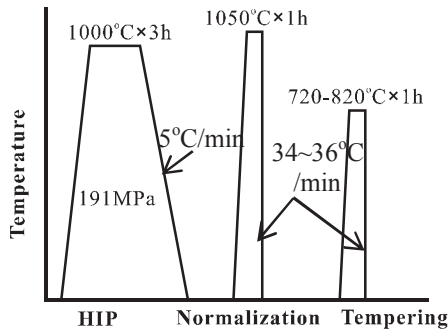


Fig. 1. HIP and PBHT procedure.

3. Results and discussion

3.1 Hardness and grain size after PBHT

Fig. 2 shows the hardness of 9Cr-ODS and JLF-1 base metals before HIP (as-received), after HIP (as-HIPed), and after PBHT. After HIP, because of the cooling rate of 5°C per minute was too slow to quench, 9Cr-ODS base metal was softened. For JLF-1 base metal, hardening occurred, on the other hand. HIP at 1000°C induced normalization and quenching for JLF-1, and produced as-quenched martensitic phase. After PBHT with normalization at 1050°C at a cooling rate of 34~36°C per minute, both 9Cr-ODS and JLF-1 base metals were quenched. After the following tempering at 720-820°C, as temperature increased, the hardness of the both decreased. Tempering at 740°C and 760°C seems to be appropriate to recover the hardness to the level similar to that before HIP.

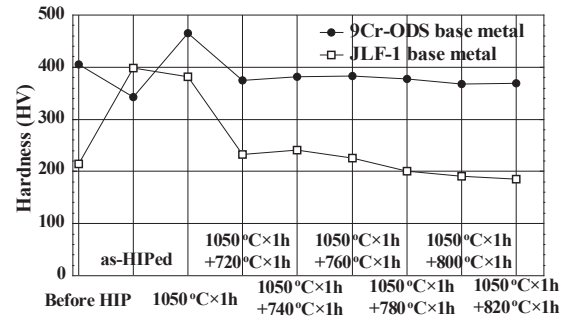


Fig. 2. Hardness of the base metals of 9Cr-ODS and JLF-1 before HIP, as-HIPed and after PBHT, reproduced from ref.[7].

Fig. 3 depicts the grain size of 9Cr-ODS and JLF-1 base metals. For 9Cr-ODS base metal, the grain size is about 1µm with no significant change after HIP and PBHT, because the high density of nano-oxide particles in the matrix could retard grain growth [10]. For JLF-1 base metal, the grain size increased after HIP, and further increased after PBHT. There are sub-grains in a prior austenite grain of RAFM steel. While tempering at high temperature, especially near the recrystallization temperature, dislocations rearranged, and the sub-grains would grow up. Thus the grain size may increase when tempering at 780°C and 800°C in this study.

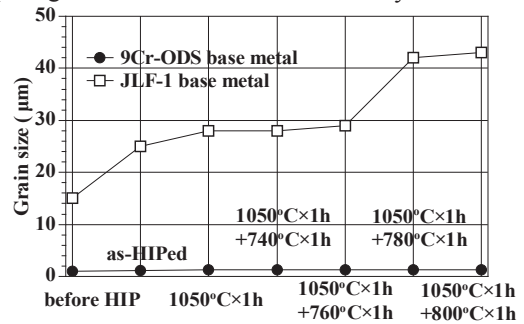


Fig. 3. Grain size evolution of 9Cr-ODS and JLF-1 base metals, reproduced from ref.[7].

3.2 Microstructure evolution of 9Cr-ODS base metal

Fig. 4 shows microstructural evolution of 9Cr-ODS before HIP, as-HIPed, and after PBHT. During the HIP and PBHT procedure, the microstructure of 9Cr-ODS base metal has changed. Before HIP, 9Cr-ODS is tempered martensitic phase, with M₂₃C₆ type of carbides [11] distributed on the grain boundaries. TEM image shows tempered martensitic laths and dislocations. There may be errors for the statistics on the size and density for the nano-oxide particles originated from the thickness estimation and imaging conditions during the TEM observation. Moreover, the nano-oxide particles may be different in different sampling area, thus further investigation is necessary to extract statistically significant changes.

However, from the preliminary rough estimate in this study, the number density of nano-oxide particles in as-received is about $1.6 \times 10^{23} \text{m}^{-3}$ with mean diameter of 7.4nm, as shown in Table 2. After HIP, the carbides, with 150-400nm in length, and 60-180nm in width, clustered on the grain boundaries. The clusters are about 150-1800nm in length. The carbides are expected to be M_3C ($\text{M}=\text{Fe}, \text{Cr}, \text{W}$) according to Fe- Fe_3C phase diagram [12]. The microstructure is ferritic phase according to CCT diagram of 9Cr-ODS [13] and the TEM image in Fig. 4(d) which shows low density of dislocations and carbide precipitates. The density of the nano-oxide particles decreased to about $1.2 \times 10^{23} \text{m}^{-3}$, with the mean diameter increased to 9.4nm. While after PBHT with normalization at 1050°C for 1h followed by tempering at 760°C for 1h, microstructure of 9Cr-ODS was recovered to tempered martensitic phase with high density of carbides, dislocations, laths, and nano-oxide particles with number density of $1.5 \times 10^{23} \text{m}^{-3}$, similar to that before HIP, but with a smaller particle size of 5.2nm.

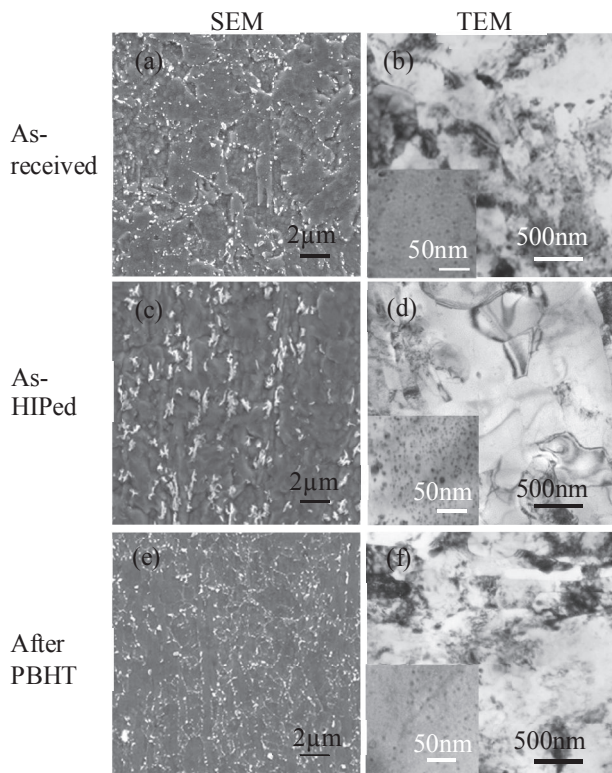


Fig. 4. Microstructure of 9Cr-ODS before HIP (a-b), as-HIPed (c-d), and after PBHT at 1050°C×1h+760°C×1h (e-f); (a, c, e)— SEM images, (b, d, f) —TEM images.

Table 2 Data of nano-oxide particles in 9Cr-ODS as-received, as-HIPed, and after PBHT at 1050°C×1h+760°C×1h.

	As-received	As-HIPed	After PBHT
Min. diameter (nm)	2	3.5	1.9
Max. diameter (nm)	23.2	39.7	20.4
Mean diameter (nm)	7.4	9.4	5.2
Density N (10^{23}m^{-3})	1.6	1.2	1.5

Fig. 5 shows the size distribution of nano-oxide particles in 9Cr-ODS base metal. Most of the nano-oxide particles in the as-received (before HIP) are in the range of 2-8nm in diameter; the maximum is about 20nm. But after HIP, the size of nano-oxide particles was about 3.5-15nm with some large particles of 40nm in diameter. Table 2 summarizes the data of the nano-oxide particles in 9Cr-ODS. It can be seen that, after HIP with a slow cooling rate, the nano-oxide particles slightly grow up with the number density decreased. After PBHT with normalization at 1050°C for 1h and tempering at 760°C for 1h, the microstructure has recovered to tempered martensitic phase. The nano-oxide particles were 1.9-7nm in diameter, the maximum is around 20nm, with size and density a little smaller than that before HIP. However, as shown in Fig. 4(c, d) and Table 3, low density dislocations in ferrite matrix and uneven distribution of coarse carbide clusters on grain boundaries may mainly contribute to the softening of the 9Cr-ODS base metal after HIP.

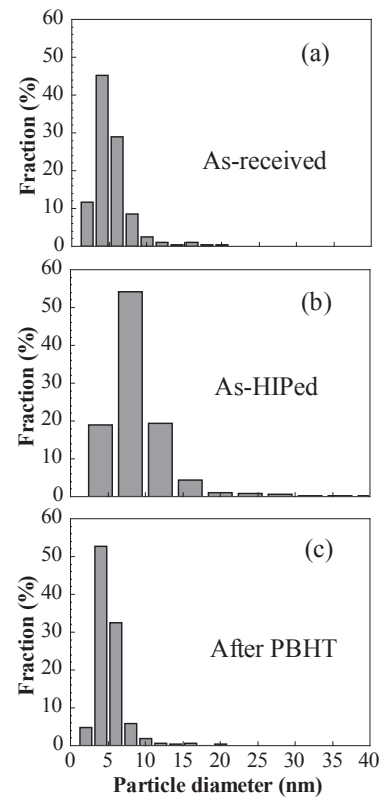


Fig. 5. Size distribution of nano-oxide particles in 9Cr-ODS base metal, (a) as-received; (b) as-HIPed; (c) after PBHT at 1050°C×1h+760°C×1h.

Table 3 Mean size of carbides in 9Cr-ODS and JLF-1 base metals

	9Cr-ODS		JLF-1	
	Condition	Size(nm)	Condition	Size(nm)
As-received	1050°C×1h+800°C×1h, AC	150	1050°C×1h+780°C×1h, AC	160
As-HIPed	1000°C×3h×191M Pa, 5°C/min	650	1000°C×3h×191M Pa, 5°C/min	—
After PBHT	1050°C×1h+760°C×1h, 36°C/min	120	1050°C×1h+760°C×1h, 36°C/min	120

3.3 Microstructure evolution of JLF-1 base metal

Fig. 6 depicts the microstructure of JLF-1 base metal. Before HIP, JLF-1 is tempered martensitic phase with laths, dislocations, and $M_{23}C_6$ carbides on lath and grain boundaries. The carbide size is shown in Table 3. While after HIP, the microstructure is quenched martensitic phase. No carbides on the lath and grain boundaries are observed, instead, MX particles and dislocation tangles form in the matrix. When PBHT with normalization and tempering was carried out, the microstructure has been recovered to tempered martensitic phase with laths, dislocations, and carbides on lath and grain boundaries. The carbide size is smaller. This may be the reason why the hardening is a little larger than that before HIP.

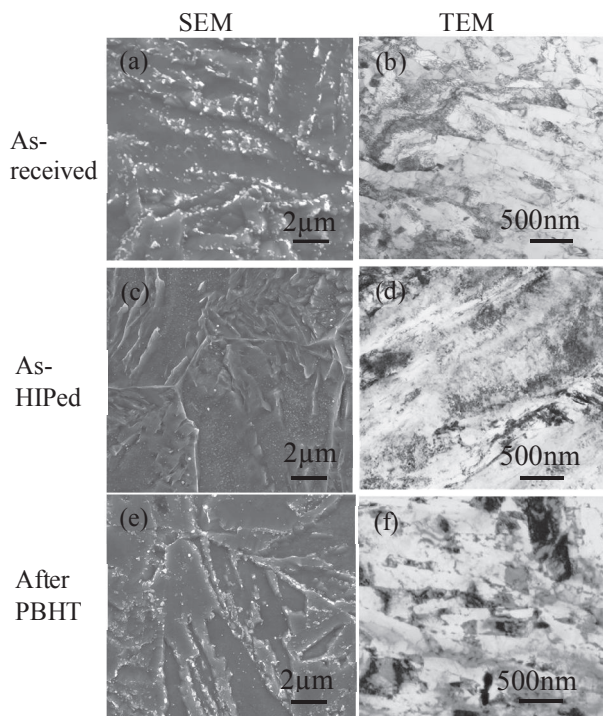


Fig. 6. Microstructure of JLF-1 before HIP (a-b), as-HIPed (c-d), and after PBHT at $1050^{\circ}\text{C}\times 1\text{h}+760^{\circ}\text{C}\times 1\text{h}$ (e-f). (a, c, e) —SEM images, (b, d, f) —TEM images.

3.4 Microstructural evolution of the interface

Fig.7 shows the interface between 9Cr-ODS and JLF-1 in the conditions of as-HIPed and after PBHT. After HIP, as depicted before in [7], coarse carbides M_3C emerge on the 9Cr-ODS side, while quenched martensitic structure appears on the JLF-1 side. However, there is a layer of grains with few MX nano-particles and no lath structure at the interface on the JLF-1 side. It seems to be ferritic structure formed during the HIP process. After PBHT with normalization and tempering, both the coarse carbides on the 9Cr-ODS side and the few-particle layer on the JLF-1 side disappear. Instead, tempered martensitic

structure with normal $M_{23}C_6$ carbides formed in the whole joint.

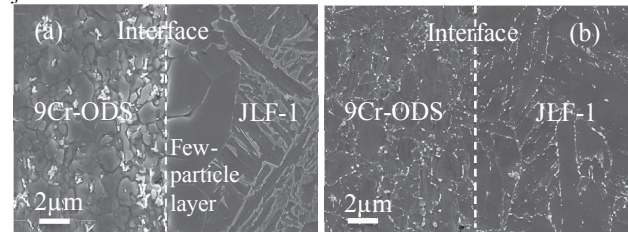


Fig.7. Microstructure of the interface in as-HIPed (a), and after PBHT at $1050^{\circ}\text{C}\times 1\text{h}+760^{\circ}\text{C}\times 1\text{h}$ (b).

4. Conclusions

A diffusion-bonded joint of 9Cr-ODS and JLF-1 was fabricated by HIP. PBHT with normalization and tempering was utilized to recover the hardness and microstructure of the joint. After HIP, the 9Cr-ODS base metal was softened because of the slow cooling rate of HIP. The microstructure was ferritic phase with low density dislocations and coarse carbides M_3C on the grain boundaries. JLF-1 base metal was hardened by the HIP treatment because quenched martensitic phase formed after HIP. While after PBHT with normalization and tempering at a fast cooling rate, hardness of both 9Cr-ODS and JLF-1 base metals was recovered to the level similar to that before HIP. The microstructure for the whole joint including the interface and the base metals was tempered martensitic structure with $M_{23}C_6$ carbides.

Acknowledgements

This work was supported by NIFS budget codes NIFSUFF024 and NIFSKOBF020.

References

- [1] S. Ukai, *et al.*, *J. Nucl. Mater.* **307–311**, 749 (2002).
- [2] Y. Li, *et al.*, *Fusion Eng. Des.* **86**, 2495 (2011).
- [3] L. Commin, *et al.*, *J. Nucl. Mater.* **442**, S552 (2013).
- [4] T. Uwaba, *et al.*, *J. Nucl. Mater.* **367–370**, 1213(2007).
- [5] D.T. Hoelzer, *et al.*, *J. Nucl. Mater.* **442**, S529 (2013).
- [6] S. Noh, *et al.*, *J. Nucl. Mater.* **426**, 208 (2012).
- [7] H.Y. Fu, *et al.*, *Fusion Eng. Des.* **89**, 1658 (2014).
- [8] T. Muroga, *et al.*, *Fusion Eng. Des.* **89**, 1717 (2014).
- [9] A. Kohyama, *et al.*, *J. Nucl. Mater.* **258–263**, 1319 (1998).
- [10] J. Gan, *et al.*, Report of Idaho National Laboratory, 2007.
- [11] J.K. Goddard, *Characterization of two ODS alloys: 18Cr ODS and 9Cr ODS* (Theses and Dissertations for University of South Carolina, 2013) P.29.
- [12] W.D. Callister, *Fundamentals of Materials Science and Engineering* (An Integrated Approach, 4 edition, Wiley, Hoboken, N.J, 2012) P.303.
- [13] S. Ukai, *Oxide Dispersion Strengthened Steels-Compr. Nucl. Mater.*, (Elsevier, Oxford, 2012) P. 241.